PAPER • OPEN ACCESS

Increased extreme humid heat hazard faced by agricultural workers

To cite this article: Connor D Diaz *et al* 2023 *Environ. Res. Commun.* **5** 115013

Environmental Research Communications

PAPER

Increased extreme humid heat hazard faced by agricultural workers

Connor D Diaz[1,2,3], **Mingfang Ting**[3,4], **Radley Horton**[3,4], **Deepti Singh**[5], **Cassandra D W Rogers**[5,6] and **Ethan Coffel**[7]

[1] Department of Earth and Environmental Sciences, Columbia University, New York, NY, United States of America
[2] Department of Applied Physics and Applied Mathematics, Columbia University, New York, NY, United States of America
[3] Lamont-Doherty Earth Observatory, Columbia University, 61 Rt. 9W, Palisades, NY 10964, United States of America
[4] Columbia Climate School, Columbia University, New York, NY, United States of America
[5] School of the Environment, Washington State University, Vancouver, WA, United States of America
[6] Bureau of Meteorology, Melbourne, VIC, Australia
[7] Department of Geography and the Environment, Syracuse University, Syracuse, NY, United States of America

E-mail: connor.diaz@columbia.edu

Keywords: heat stress, humid heat, agricultural workers, crop impacts, food system, climate variability, potential worker exposure

OPEN ACCESS

RECEIVED
31 March 2023

REVISED
12 September 2023

ACCEPTED FOR PUBLICATION
11 October 2023

PUBLISHED
20 November 2023

Abstract

Increases in population exposure to humid heat extremes in agriculturally-dependent areas of the world highlights the importance of understanding how the location and timing of humid heat extremes intersects with labor-intensive agricultural activities. Agricultural workers are acutely vulnerable to heat-related health and productivity impacts as a result of the outdoor and physical nature of their work and by compounding socio-economic factors. Here, we identify the regions, crops, and seasons when agricultural workers experience the highest hazard from extreme humid heat. Using daily maximum wet-bulb temperature data, and region-specific agricultural calendars and cropland area for 12 crops, we quantify the number of extreme humid heat days during the planting and harvesting seasons for each crop between 1979–2019. We find that rice, an extremely labor-intensive crop, and maize croplands experienced the greatest exposure to dangerous humid heat (integrating cropland area exposed to >27 °C wet-bulb temperatures), with 2001–2019 mean rice and maize cropland exposure increasing 1.8 and 1.9 times the 1979–2000 mean exposure, respectively. Crops in socio-economically vulnerable regions, including Southeast Asia, equatorial South America, the Indo-Gangetic Basin, coastal Mexico, and the northern coast of the Gulf of Guinea, experience the most frequent exposure to these extremes, in certain areas exceeding 60 extreme humid heat days per year when crops are being cultivated. They also experience higher trends relative to other world regions, with certain areas exceeding a 15 day per decade increase in extreme humid heat days. Our crop and location-specific analysis of extreme humid heat hazards during labor-intensive agricultural seasons can inform the design of policies and efforts to reduce the adverse health and productivity impacts on this vulnerable population that is crucial to the global food system.

1. Introduction

The effects of climate change are not distributed uniformly across the globe, and as warming continues, certain regions and communities will experience disproportionately more hazards and impacts (Ranasinghe *et al* 2021, U.S. Environmental Protection Agency 2021, Sun *et al* 2015, Forzieri *et al* 2018, Wang *et al* 2020). Among these changing hazards is that posed by extreme humid heat, which is the combined effect of high dry-bulb air temperature and high humidity and is often quantified by wet-bulb temperature (T_W). The frequency of humid heat extremes has increased substantially in the past four decades over densely-populated and socio-economically vulnerable regions of the world at a faster rate than dry heat extremes, with a person on average experiencing about five more extreme humid heat days each decade (Rogers *et al* 2021). Future population exposure to T_W exceeding 32°C, a threshold indicating potential adverse human health effects, is projected to increase 5 to 10-fold by the 2070s under different emissions scenarios due to dangerous humid heat becoming

much more frequent (Coffel *et al* 2017), especially in densely-populated regions where current humid heat levels are already high (Rogers *et al* 2021). These increases will be especially large in the tropics (Wang *et al* 2020, Rogers *et al* 2021) and are also projected to last longer, and increase in intensity under global warming (Wang *et al* 2020).

Increases in T_W pose a substantial risk to human health, yet historical changes and their impacts are not well understood. When combined with high dry-bulb temperatures, high specific humidity decreases the bodys ability to cool by sweating, exacerbating heat stress (Osilla *et al* 2022). Sherwood and Huber (2010) suggest a theoretical lethal T_W limit of 35 °C based on a thermodynamic gradient from the core human body temperature to the ambient environment. However, recent experimental work by Vecellio *et al* (2021) suggests that this limit varies based on local climatological conditions and is potentially much lower than 35 °C T_W. At T_W of approximately 27 °C, heat stress shifts from demanding extreme caution to being dangerous for human health (Kang and Eltahir 2018 [table S6]; National Weather Service, n.d.). Additionally, Hanna and Tait (2015) note that while humans have the capability to acclimatize to increasingly hot environments, climate change will introduce extreme T_W conditions in which even highly acclimatized individuals, like outdoor workers, will not be able to sustain physical activity outdoors.

Agricultural workers are a population especially vulnerable to a proliferation of extreme humid heat events as they work outdoors for extended periods and often undertake strenuous physical labor. They are also among the most socio-economically vulnerable populations (Ergon Associates 2016). Frameworks have been developed that contextualize agricultural workers' risk of heat-related illness by examining the specific environmental exposures they face, the details of their physiological response and sensitivity to heat, possible adaptive measures that can reduce risk, as well as the sociological factors that increase their vulnerability (Mac and McCauley 2017). Riley *et al* (2018) have shown that United States counties with higher proportions of outdoor workers see more emergency room visits and hospitalizations during heat wave events than other counties. Similarly, recent work shows that chronic kidney disease in Central America has been linked to heat stress experienced while harvesting sugarcane (Wesseling *et al* 2020). Additionally, Spector *et al* (2016) found that agricultural workers in Washington state have a higher probability of traumatic injury during hot and humid days, especially during the summer harvest season. Recent modeling shows that even under moderate warming scenarios, heat risks to US agricultural workers are projected to increase, along with the number of days in agricultural regions that are classified as unsafe for outdoor work (Tigchelaar *et al* 2020). Consequently, modeling by de Lima *et al* (2021) projected large reductions in the productivity of agricultural workers in some regions, with limited potential for offsets via adaptation strategies, such as changing the time of day of agricultural labor.

Given the substantial impacts extreme humid heat poses to the health and productivity of agricultural workers and the global food system, it is imperative that we better understand the risks that extreme T_W poses to these vulnerable populations around the world. Our study builds upon the limited research to date that links humid heat extremes to the heat stress hazards faced by agricultural workers, integrating an understanding of physiologically hazardous heat with data on the timing of agriculture across the world. First, we compute a global climatology of dangerous humid heat exposure over land, then, using crop-specific and region-specific agricultural calendars, we examine cropland exposure to humid heat during periods of the agricultural season when workers are likely to be in the field performing strenuous activities. Cropland exposure during labor-intensive agricultural seasons is used as a proxy for agricultural worker exposure, which we refer to as potential worker exposure. Next, focusing on rice and maize, we analyze the seasonality (planting or harvest season) of this exposure and consider annual trends in overall labor-intensive season exposure over the study period. Lastly, we examine the impact of the El Niño Southern Oscillation (ENSO) on dangerous humid heat extremes over land in order to consider its role on potential worker exposure. Our work makes novel contributions to understanding the spatial and temporal distribution of humid heat hazards to agricultural workers across the world by linking the timing and location of agricultural activity with extreme daily T_W using both absolute ($T_W > 27$ °C) and relative (local 95th percentile of T_W) thresholds for 12 different crops.

2. Data and methods

We use three primary datasets in this analysis: (1) daily maximum T_W data produced by Rogers *et al* (2021) using ERA5 reanalysis data (Hersbach *et al* 2020); the authors used the Davies-Jones method (Davies-Jones 2008) as implemented by Kopp (2020) and Buzan *et al* (2015) to calculate T_W; (2) the Global Crop Calendar Dataset - a gridded dataset of planting and harvest season dates for major global crops (Sacks *et al* 2010); and (3) harvested area from Monfreda *et al* (2008). The agricultural season dates were collected as benchmarks in the 1990s and early 2000s (Sacks *et al* 2010) while the harvested area data were estimated for the year 2000 (Monfreda *et al* 2008); these data are thus time invariant for this analysis.

We analyze the occurrence of extreme humid heat days during the crop-specific planting and harvest seasons, both individually and combined (hereafter referred to as the labor season), using the planting and

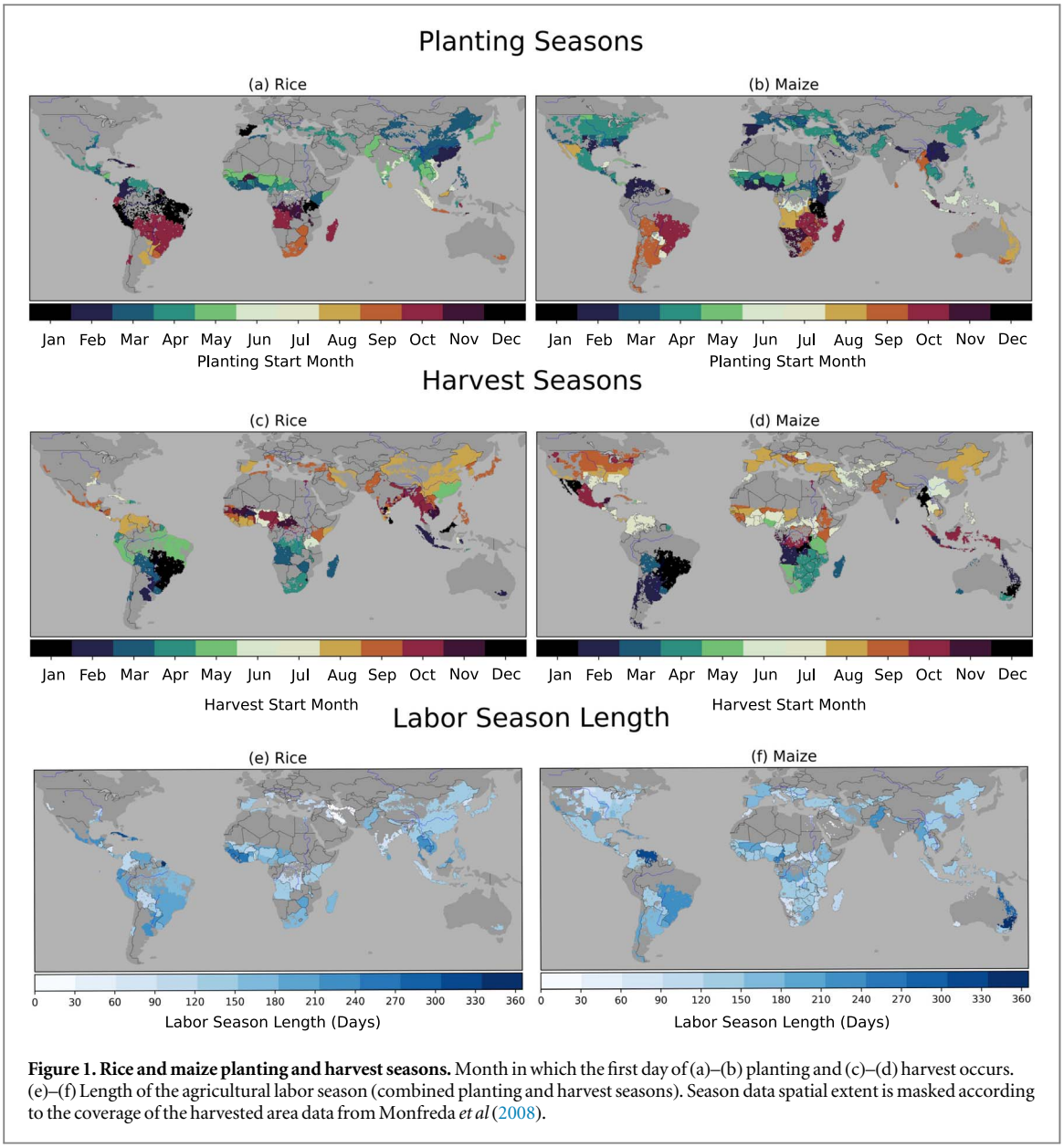

Figure 1. Rice and maize planting and harvest seasons. Month in which the first day of (a)–(b) planting and (c)–(d) harvest occurs. (e)–(f) Length of the agricultural labor season (combined planting and harvest seasons). Season data spatial extent is masked according to the coverage of the harvested area data from Monfreda *et al* (2008).

harvest season dates from the Global Crop Calendar Dataset over the 1979–2019 period. This dataset provides beginning and ending planting and harvest season dates for each crop in each grid cell where the crop is harvested, these delimit the seasons for our analysis. An example of the planting and harvest seasons for rice and maize as tabulated in the Global Crop Calendar Dataset is shown in figure 1. For most of the regions, planting season for both crops (figures 1(a), (b)) starts in late winter and early spring, and harvest season (figures 1(c), (d)) falls between late summer and autumn. The labor seasons shown in figures 1(e), (f) tend to last four or more months for most rice and maize growing regions. The reasons for the papers focus on rice and maize are explained in Results section 3.2.

Two thresholds are used to define extremes: an absolute threshold of 27 °C daily maximum T_W (T_W^{27c}), a threshold considered to be dangerous to outdoor workers (Kang and Eltahir 2018, National Weather Service, n.d.), and a relative threshold defined as the local (grid cell) 95th percentile of daily maximum T_W over 1979-2019 (T_W^{95p}). The inclusion of the relative threshold allows us to investigate local humid heat extremes in relatively cooler regions that do not often exceed T_W^{27c}, and hence could pose health risks to communities not acclimatized to such conditions. It also allows us to investigate extreme conditions in regions where humid heat extremes are often higher than T_W^{27c}.

The total number of days exceeding T_W^{27c} and T_W^{95p} are calculated for each year over each land grid cell of the Global Crop Calendar Dataset (0.5° × 0.5°), which requires a regridding of the 0.28125° × 0.28125° ERA5 data. Extreme humid heat days for each grid cell are then aggregated to their corresponding crop-specific agricultural season. Grid cells that do not overlap with the harvested area cells of the crop from Monfreda *et al* (2008) are

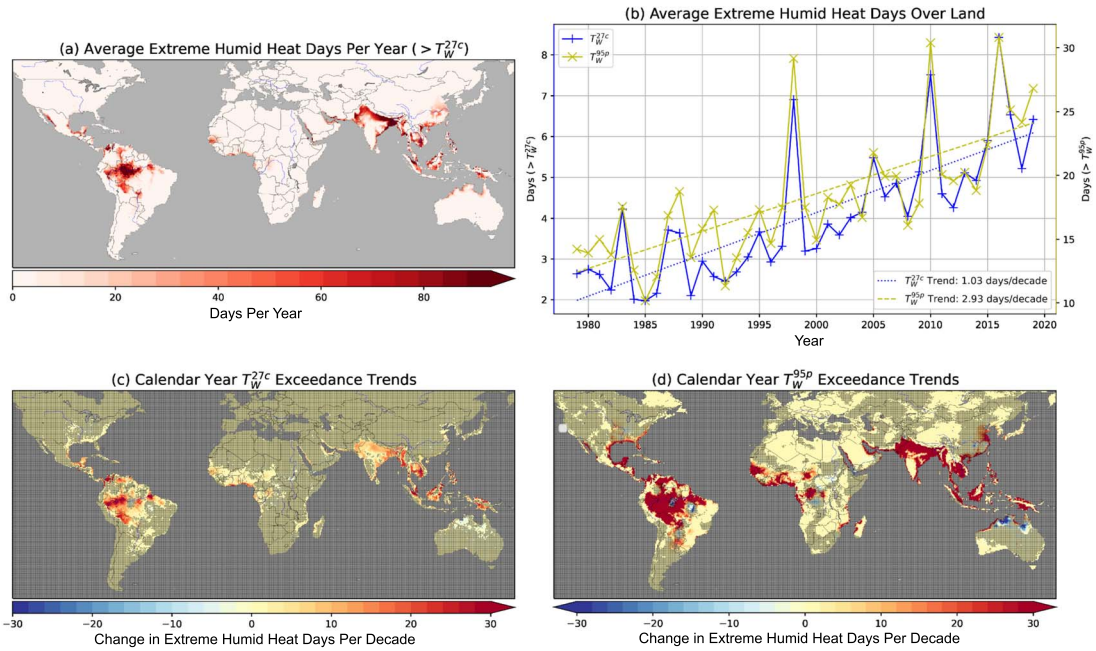

Figure 2. Climatology and trends in extreme humid heat frequencies. (a) Number of days per year exceeding T_W^{27c} over land; note that the color bar saturates at 93 days (~3 months). (b) Area-weighted average T_W^{95p} exceedances (yellow x markers, right y-axis) and T_W^{27c} exceedances (blue + markers, left y-axis) Note the different vertical axes for T_W^{27c} and T_W^{95p} exceedances. Averages are calculated over land only. Trends are significant at the 95% confidence level using the Mann-Kendall test (p-values <0.001). Dotted blue and dashed yellow lines show linear trendlines for T_W^{27c} and T_W^{95p}, respectively. Linear trends in annual days exceeding (c) T_W^{27c} and (d) T_W^{95p}. Hatching indicates trends that are not significant at the 95% confidence level using the Mann-Kendall test (p-values <0.001).

masked. This procedure is similar to that of Gourdji *et al* (2013), who investigated exceedances of dry-bulb temperatures dangerous to certain crops during their reproductive seasons.

We also analyze the relationship between El Niño-Southern Oscillation (ENSO) conditions and land exposure to dangerous humid heat, based on the NOAA Oceanic Niño index (ONI; Huang *et al* 2017). This dataset yields nine El Niño events, defining an event by 5 consecutive 3-month running mean ONIs categorized as such: four moderate events ($1.5 > ONI \geqslant 1.0$; 1986/87, 1994/95, 2002/03, 2009/10) and five strong events ($ONI \geqslant 1.5$; 1982/83, 1987/88, 1991/92, 1997/98, 2015/16).

3. Results

3.1. Climatology and trends in humid heat extremes

We first examine global land regions where extreme humid heat events, as defined by our physiologically-based thresholds, tend to occur frequently and identify trends over the past several decades (figure 2). Figure 2(a) reveals that some land areas experience three or more months of T_W temperatures exceeding 27 °C ($> T_W^{27c}$) per year on average. These regions include the Amazon, the Indo-Gangetic Basin, Northern Colombia, the Mexican coast, the coasts of the Red Sea and Persian Gulf, Southeast Asia, and the Maritime continent. The northern coast of the Gulf of Guinea, Senegal and the Gambia, and the northern coast of Australia also experience approximately two months of extreme humid heat. While the majority of these locations are in the tropics and are near-coastal, there are several sub-tropical and inland exceptions, such as northern South Asia, and northeastern and southeastern China.

Averaged over global land areas, exceedances of T_W^{27c} more than doubled over 1979-2019, from ~2–4 days of extreme humid heat per year in the 1980s to ~4–8.5 days in the 2010s (figure 2(b)), an increase of ~1 day per decade. In comparison, global exceedances of the local 95th percentile show a stronger increase of ~3 days per decade. Both of these trends are statistically significant as described in figure 2. Both extreme humid heat indices show peaks during strong El Niño years, particularly 1998, 2010 and 2016. While the 1983 and 1987 El Niño events also show a relatively high number of extreme humid heat days, they are less marked relative to the surrounding non-El Niño years. The differing influence of various El Niño events could be due to a number of factors, including duration, timing, peak strength, and interactions with the mean warming trend.

Many regions with a climatologically high number of extreme T_W days per year ($> T_W^{27c}$, figure 2(a)) also show large positive trends in exceedances of this metric (figure 2(c)). Trends in T_W^{95p} exceedances, more

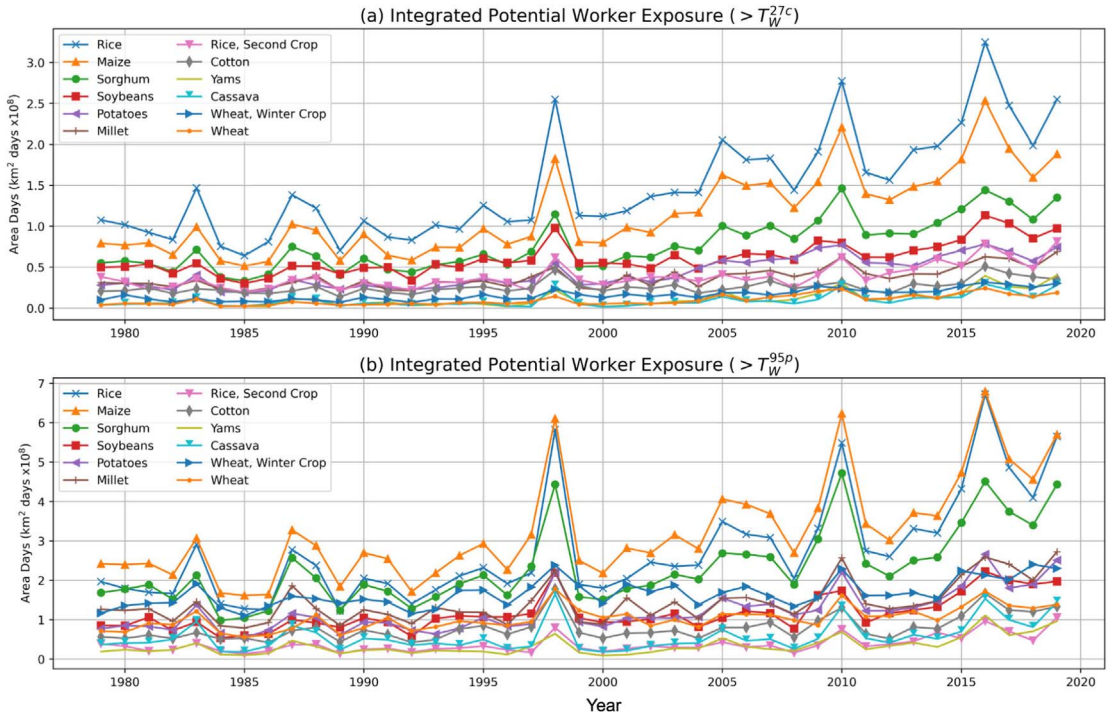

Figure 3. Integrated potential worker exposure to extreme humid heat. Cropland area in each grid-cell (km^2) multiplied by the number of days in the agricultural labor season exceeding (a) T_W^{27c} and (b) T_W^{95p} for each grid-cell. Area days are in hundred million square kilometer days.

surprisingly, exhibit a similar pattern (figure 2(d)) despite by definition featuring the same number of days everywhere in the climatology. The largest increases occur in some of the most densely populated regions in the world, such as the Mekong Delta, and Bangladesh/West Bengal, with large increases also found in parts of the Amazon, northern Colombia, and the Maritime Continent. T_W^{95p} exceedance trends are stronger and extend over a greater geographic region, with relatively weak yet significant trends extending to cooler mid- and high-latitude land regions. Overall, the consistency of the exceedance trends for both thresholds reveals increases in extreme T_W exposure over many land regions. In contrast, very few regions see decreases in extreme T_W exposure (e.g. parts of northern Australia, figure 2(d)). Figure 2 is restricted to three regions of interest, Central/South America, South Asia and the Maritime Continent, and the Gulf of Guinea in figures A1, A2, and A3.

3.2. Integrated potential worker exposure to humid heat during the agricultural labor season

To identify crops whose workers are subject to the greatest potential exposure to humid heat during the labor-intensive seasons (figure 1), we multiplied the cropland area in each grid cell by the number of extreme T_W days exceeding the threshold values for each crops season, then integrated this across all grid cells (figure 3). We use this cropland exposure as a proxy for potential exposure of crop workers, as there are no comprehensive data on the times of day various crop workers are in the field. All original 25 crops in the Global Crop Calendar Dataset were analyzed with this metric; the 12 crops with the highest consistent values across both thresholds are shown in figure 3. This aggregated measure of exposure depicts the effect of both the extent of area exposed and the frequency of humid heat exposure for each crop across the globe, with the assumption of constant cropland area from 1979-2019. This likely leads to an underestimate, given the expansion of global cropland in the 21st century, notably in South America (Potapov *et al* 2021). Using T_W^{27c}, rice, maize, sorghum, and soybeans are the crops whose workers are the most potentially exposed to extreme T_W (figure 3(a)). We also examined potential worker exposure using T_W^{95p} to capture potential impacts from locally extreme conditions (figure 3(b)). While rice, maize, and sorghum have the greatest potential worker exposures to humid heat for T_W^{95p} (figure 3(b)), consistent with T_W^{27c}, soybean exposure is lower relative to other crops for T_W^{95p} than for T_W^{27c}. Additionally, maize exposure for T_W^{95p} exceeds that for rice, whereas the opposite is true for T_W^{27c}. This discrepancy occurs because maize is more common than rice in temperate areas that rarely exceed T_W^{27c} (figures 1(e), (f) and 2(a)). For both thresholds there is a strong ENSO signal in potential worker exposure, particularly for 1998, 2010, and 2016 (figure 3). This reflects the ENSO signal in humid heat frequencies (figure 2(b)). Because figure 3 indicates that rice and maize agricultural workers are the most potentially exposed, we focus the remainder of our detailed analysis on these two crops.

Potential worker exposure for rice and maize nearly doubled during the study period, with the mean for the latter half of the period (2001-2019) being 1.8 times (rice) and 1.9 times (maize) greater than those for the earlier period (1979-2000). For rice, this is a 1979–2000 mean of ∼1.08 hundred million area days and a 2001-2019 mean of ∼1.94 hundred million area days.

3.3. Potential worker exposure for rice and maize

Given their large increases in potential exposure (figure 3), we examine the spatial and temporal distribution of humid heat extremes for rice and maize. Both rice and maize are widely cultivated, with rice dominant in Asia, South America, and central Africa, whereas maize is prevalent in North America, southern South America, and southern Africa. Rice cropland in this dataset covers 35.8 million square kilometers and maize 43.5 million square kilometers. As shown in figure 1, planting of both rice and maize outside the tropics starts in late winter and early spring, and the harvest season starts ∼2–4 months later. Maize planting and harvest seasons for countries in Southeast Asia and the Maritime Continent differ more from their neighbors than those in the mid-latitudes. For example, regions of Myanmar plant maize in September, while regions in Thailand plant in April and parts of Sumatra plant in November, with similarly disjointed harvest seasons (figures 1(a), (b), (c), (d)). The total labor season for rice and maize is generally less than ∼7 months (figures 1(e), (f)). Regions with notably long labor seasons covering most of the year are all in the tropics, including Cuba and French Guiana (rice, figure 1(e)), and Venezuela and eastern Australia (maize, figure 1(f)).

Figure 4 shows the potential worker exposure to extreme humid heat for rice and maize in terms of the average days exceeding the threshold values (figures 4(a), (b)), their trend over the last 4 decades (figures 4(c), (d)), and the relative potential exposure in the planting versus the harvest seasons (figures 4(e), (f)). (Figure 4 is restricted to the three regions of interest, Central/South America, South Asia and the Maritime Continent, and the Gulf of Guinea in figures A4, A5, and A6). For rice, the highest potential worker exposure during the labor season occurs in Bangladesh, with more than 60 days of extreme humid heat $> T_W^{27c}$ (figure 4(a)). Other regions with relatively high frequencies include the Mekong Delta, coastal Thailand, the Irrawaddy River Delta in Myanmar, the Maritime Continent, and parts of coastal Mexico and the Amazon, which show 30 or more days of extreme humid heat $> T_W^{27c}$ (figure 4(a)). Positive trends in potential worker exposure (figure 4(c)) are observed where extreme heat frequencies are already high for rice, with strong trends occurring in Southeast Asia and parts of the Amazon ($\geqslant$10 days per decade).

For the maize labor season, the highest potential worker exposure occurs across much of Pakistan and parts of Mekong Delta (figure 4(b)). Other regions with high potential worker exposure include northern Colombia and Venezuela, the Philippines, parts of coastal Mexico, and coastal Iran (figure 4(b)). The strongest positive trends are found in northern Colombia, Venezuela, and the Mekong Delta, which also have high humid heat frequencies similar to the rice frequency trends at $\geqslant$10 days per decade (figures 4(b), (d)). Figures 4(e)–(f) indicates regional patterns in which season more potential worker exposure occurs. In general, Southeast Asia, India, Pakistan, and the northern coast of the Gulf of Guinea are more exposed in the planting season for both rice and maize. eastern China and the Maritime Continent are generally more exposed in the harvest season for both crops. Regional patterns are less clear for South America, Sub-Saharan Africa, Mexico, and the southern United States where the season of more frequent potential worker exposure depends on the specific crop, and shows more small-scale spatial variability. These patterns are also shown in the frequency, trend, and seasonal bias maps for Sorghum in figure A7.

These seasonal findings are consistent with the peak timing of humid heat extremes in Rogers *et al* (2021). For example, the authors identify May as having the highest frequency of extreme T_W^{95p} days over Cambodia and Thailand, while we similarly identify this month as the start of the season with the most frequent T_W^{27c} exposure.

Area calculations from figures 4(e)–(f) shown in figure 5 also indicate that extreme humid heat exposure tends to occur more frequently during the harvest season (total area values in km^2 are tabulated in table A1). For rice, 10.1 million square kilometers of cropland are more exposed in the harvest season, compared to 7.8 million square kilometers more exposed in the planting season. These exposures represent 30.5% and 22.3% of total rice cropland, respectively. For maize, 12.2 million square kilometers are more exposed in the harvest season than in the planting season, and 5.7 millions square kilometers are more exposed in the planting season than the harvest season, representing 28.1% and 13.1% of total maize cropland. Regions where potential exposure is biased towards one season over the other generally show a strong bias in that season. Considering areas where exposure is strongly biased towards a season (where there are at least twice as many mean exposures in one season over the otherratio $<$0.5 for strong harvest exposure or ratio $>$2 for strong planting exposure) ∼22% of both croplands experience strongly biased exposure in the harvest season, which is notably large considering ∼30% of the croplands are generally more exposed (ratio $<$1) in the harvest season. Similarly, 16.6% percent of rice cropland exposure is strongly biased towards the planting season (compared to 22.3% generally more exposed, ratio $>$1, in the planting season), and 9.2% of maize cropland exposure is strongly biased towards the planting season (compared to 13.1% generally more exposed in the planting season).

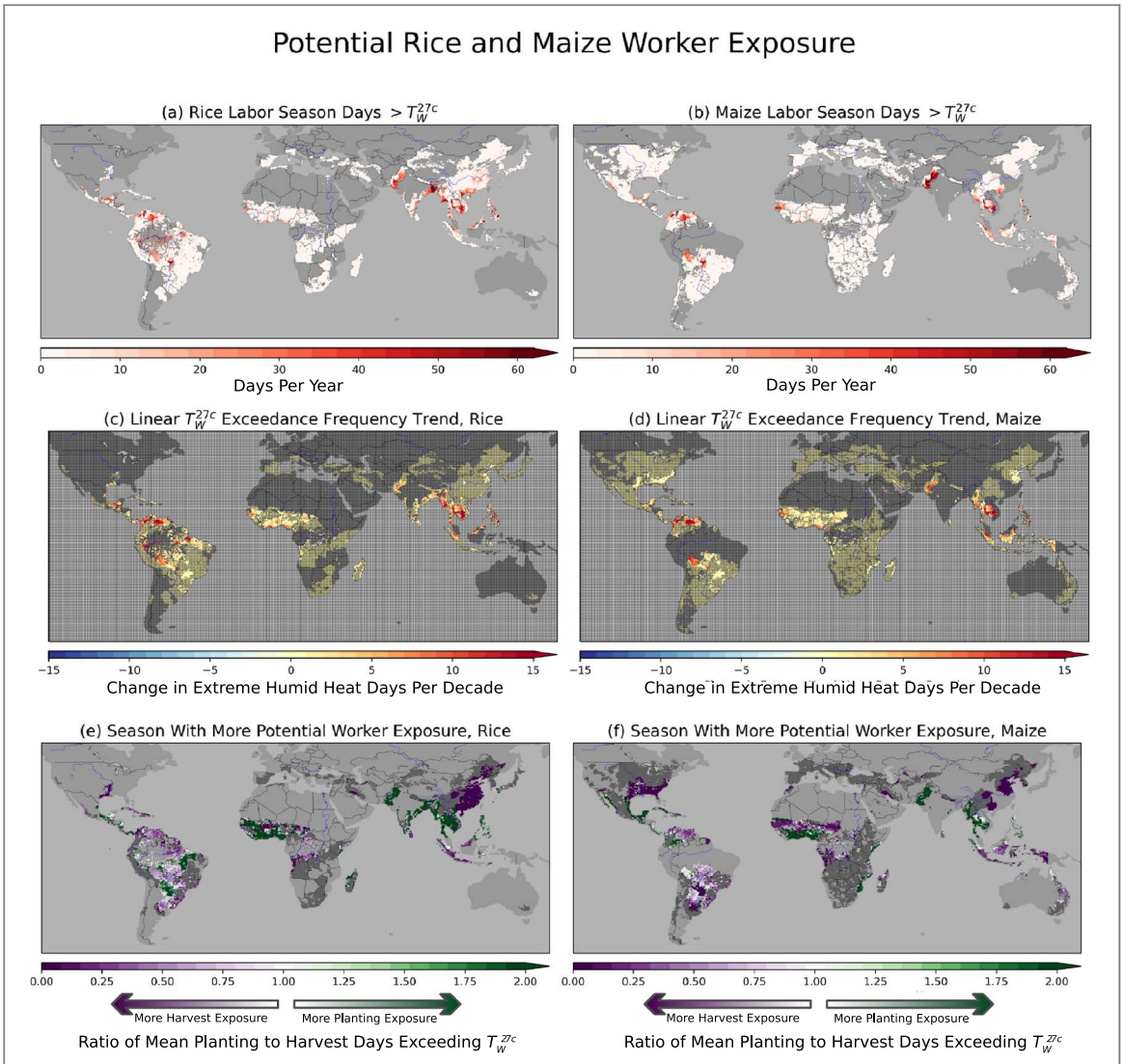

Figure 4. Spatial distribution of potential worker exposure in the labor season for rice and maize. Mean number of extreme humid heat days during the labor season exceeding the absolute threshold T_W^{27c} for (a) rice and (b) maize. Linear trends in the number of labor season days per decade exceeding T_W^{27c} for (c) rice and (d) maize. Hatching shows where trends are not significant using the Mann-Kendall test at the 95% confidence level (p-values < 0.001). Ratio of the mean number of humid heat days exceeding T_W^{27c} in the planting season to those in the harvest season for (e) rice and (f) maize. Values >1 (green, right) show more potential worker exposure in the planting season, values <1 (purple, left) show more potential worker exposure in the harvest season. Areas with no humid heat days in either season are masked in dark grey; areas with no humid heat days in the harvest season, but $\geqslant 1$ day in the planting season are reported as a ratio of >2, where the colorbar saturates.

More rice cropland is exposed in the planting season compared to maize. About 30% of both croplands are more exposed in the harvest season, but almost twice as much rice cropland is more exposed in the planting season, by percentage of total cropland, than maize. In absolute terms, rice has ~2 million square kilometers more cropland more exposed in the planting season than maize. Considering strongly biased season exposure, about twice as much rice cropland exposure is strongly biased towards the planting season than is for maize cropland.

3.4. Humid heat extremes and the El Niño-southern oscillation

Given the high humid heat frequencies (Figure 2(b)) and high potential worker exposure (Figure 3) during El Niño years, we examine the frequency of annual extreme T_W over the nine moderate to very strong (ONI >1) El Niño events (1983, 1987, 1988, 1992, 1995, 1998, 2003, 2010, and 2016) as compared to all other years (figure 6). The years examined here are the latter years of two-year El Niño events, where figure 3 indicates the increased exposure signal. To remove the secular warming trend, extreme humid heat days have been linearly detrended before compositing the El Niño years. El Niño events are associated with enhanced T_W^{27c} exceedances over Southeast Asia, Sumatra, the Amazon, southern Pakistan, Bangladesh, and the northern coast of the Gulf of Guinea (figure 5(a)). These regions also have the highest mean humid heat frequencies for all years (figure 2(a))

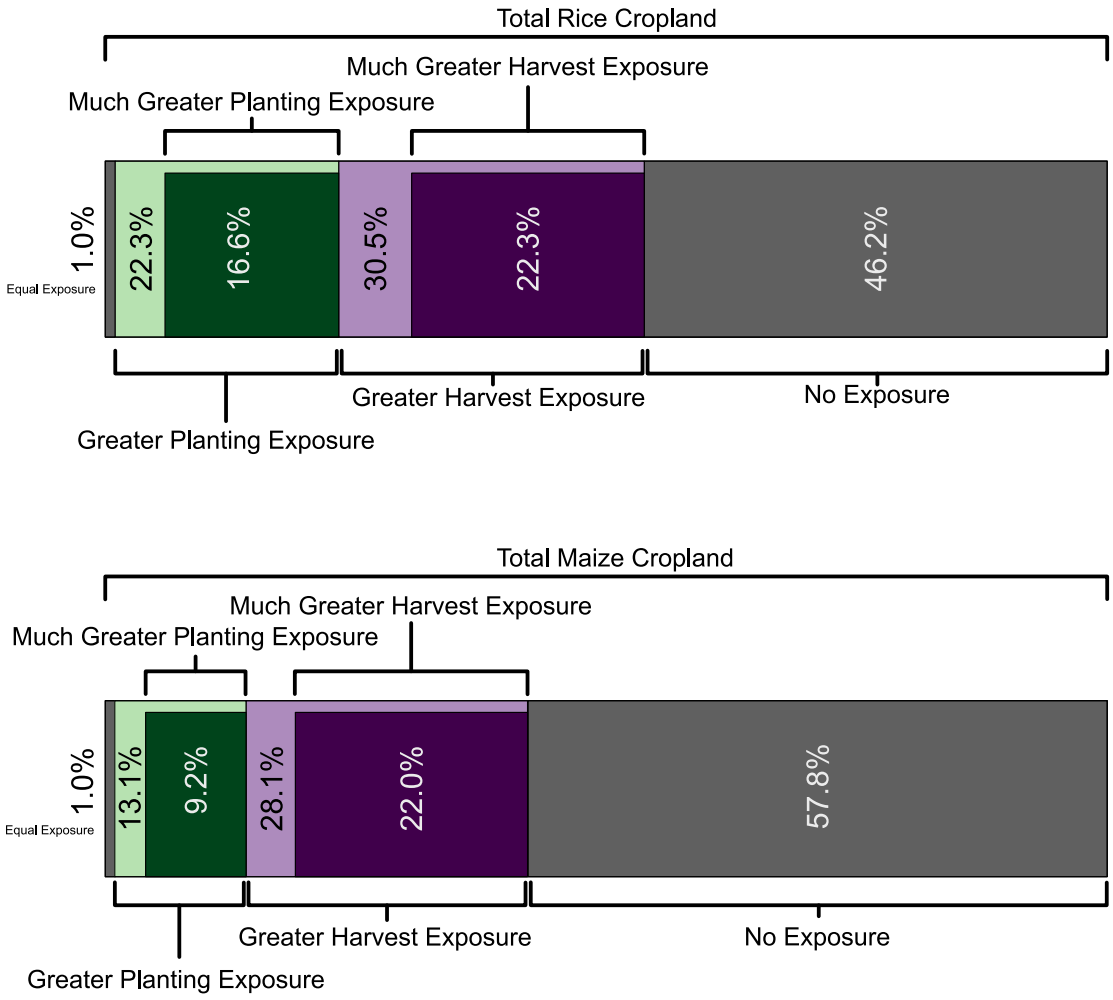

Figure 5. Breakdown of Global Rice and Maize Cropland Exposure by Season. Proportions of the total cropland exposed in the indicated season are shown. Exposed cropland is based on the climatological mean potential worker exposure calculated over the study period (1979–2019).

and high climatological potential worker exposure (figures 4(a), (b)) that have been trending upwards in recent decades (figures 4(c), (d)). Figure A8 shows figure 6 spatially restricted to only rice and maize croplands to highlight the impacts to these regions. Further, these regions also have some of the hottest T_W, the intensities of which have increased since 1979 (Rogers *et al* 2021). The relationship between El Niños and days exceeding T_W^{95p} is more geographically widespread (figure 6(b)) than the relationship to T_W^{27c}, manifesting an association between El Niños and more frequent humid heat extremes over most global land regions. Similar analysis for La Niña years shows generally opposite impacts and is shown in figure A9.

Thus, our analysis indicates that during an El Niño event, many agricultural regions are likely to experience higher exposure to T_W extremes, exacerbating the already dangerous T_W conditions that many agricultural workers already face.

4. Summary and discussion

In this study, we characterize the climatology and trends in potential agricultural worker exposure to hazardous humid heat conditions across regions for various key crops based on the crop-specific timing of planting and harvest activity. Increases in extreme humid heat frequencies over croplands during the agricultural labor seasons imply that agricultural workers will be more at risk from these events. Our use of crop and location-specific agricultural season calendars highlights large differences in humid heat exposure across crops and locations. Consistent with prior historical analyses (Raymond *et al* 2020, Rogers *et al* 2021) and projections (Coffel *et al* 2017) over the calendar year, we find the highest baseline frequency and trends in humid heat days

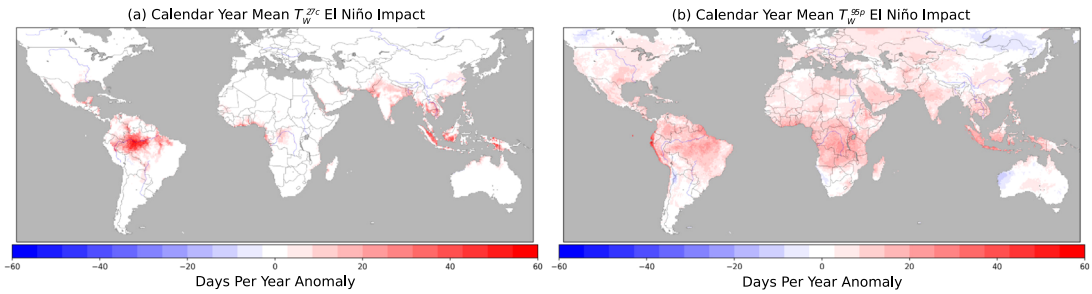

Figure 6. Mean humid heat frequency anomalies during El Niño events. Composites of the anomalous annual number of extreme humid heat days for (a) T_W^{27c} and (b) T_W^{95p}, during years with moderate to very strong ONI El Niño events (1983, 1987, 1988, 1992, 1995, 1998, 2003, 2010, and 2016). Composites are calculated after removing background linear trends in extreme humid heat day frequencies. Composites are produced using data for the entire calendar year.

occur in the tropics and lower subtropics. We find that for many crops, the area extent and frequency of potential agricultural worker exposure is increasing rapidly, particularly in the past ~15 years (figure 3).

Rice, maize, sorghum and soybean croplands are the most exposed to dangerous humid heat, and thus, in this analysis, represent the most hazardous croplands where agricultural workers may face dangerous T_W conditions. In particular, rice and maize planting seasons in Southeast Asia, coastal Mexico, the northern coast of the Gulf of Guinea, and Pakistan experience greater impacts; whereas, impacts are higher during the harvest seasons in South America, eastern China, and the Maritime Continent. We also find that El Niño conditions dramatically increase cropland exposure to dangerous humid heat, particularly since the 1997/98 El Niño. The regions of increased dangerous humid heat frequencies during El Niño years also have high climatological frequencies and trends. This emphasizes the need to better understand the influence of natural climate variability modes and their interactions with the mean warming trends to characterize and predict threats to vulnerable agricultural workers that are a backbone of the global food system.

Further, there are several fertile avenues for further research on impacts and potential adaptation strategies. First, the actual exposure and vulnerability of agricultural workers may differ dramatically from our first-order estimates based on a single humid heat metric and two extreme thresholds. The compound effects to agricultural workers from exposure to consecutive humid heat extremes during heat waves, for example, is one critical component not examined in this work. Second, our assumption that crop calendars, crop density, and worker distributions are stationary and spatially homogeneous below the regional scale shown in figure 1 also limits the generalizability of our results, as they are all dynamic variables. Future research should thus explore factors including the intensity of the labor, the number of workers, their degree of vulnerability (based on factors including pre-existing health conditions, gender, age, access to cooling for recovery when not farming, access to technological innovations such as air-conditioned tractors, work compensation structure such as piece-rate work, and local labor rights and protections), time of day of exposure to humid heat, shifting crop calendars, the regional proliferation and recession of agriculture, and factors such as solar radiation, surface winds, and exposure to humid heat thresholds higher than 27 °C T_W. Efforts toward a comprehensive census of agricultural workers would greatly improve our ability to refine the details of humid heat hazards to these vulnerable populations and could help better inform public policy aimed at mitigating health risk. Third, additional research is needed to explore the indirect impacts of humid heat on crop productivity via its impacts on agricultural worker health and productivity. While inherently important, this human health and productivity information could also be integrated with direct impacts of climate change on crops (Iizumi and Ramankutty 2016, Deryng *et al* 2014). For heat specifically, direct decreases in crop productivity are found to mostly occur due to extreme dry heat (Ting *et al* 2023) associated with high dry-bulb temperatures. While it is tempting to speculate that a tendency towards humid heat might lessen negative yield impacts, the humid heat impacts on labor productivity through health impact on workers could in principle be as impactful as direct plant impacts to overall crop productivity. Additional empirical research (along the lines of de Lima *et al* 2021) and modeling are needed to fully understand the relationship between losses in labor productivity and crop yield impacts. The potential for deleterious feedback on food security between direct damage to crops and workers in a warming world enhances the urgency of this research. Fourth, ours and others findings hint at proximity to water, whether warm water bodies and coastlines (Raymond *et al* 2022), or river valleys and irrigated land (Monteiro and Caballero 2019, Krakauer *et al* 2020, Thiery *et al* 2017) as drivers of humid heat. Since agriculture also often leverages this same proximity to water, future research should explore whether proximity of croplands to water influences worker humid heat exposure in ways not captured here. Indeed, the intensification and expansion of

agriculture in water-rich regions like the Amazon (Simon and Garagorry 2005) may already be increasing both the frequency of, and agricultural worker exposure to, dangerous humid heat, as has been suggested for the Indo-Gangetic and Indus Basins (Mishra *et al* 2020, Krakauer *et al* 2020). This possibility is hinted at by our findings of strong trends in humid heat days in regions like the Amazon and Southeast Asia, but more research is needed. The possibility that irrigation may change the timing of agricultural activity, and thus the seasons in which crop workers are engaged in outdoor work, must also be considered in future work.

Our research clearly shows that climate change, interacting with modes of natural variability such as ENSO, is already increasing the exposure of agricultural croplands, and thus highly vulnerable agricultural workers, to extreme humid heat. Not only are these workers essential to the global food system, but their livelihoods are threatened in the face of such increasing health hazards. Our initial effort here at identifying crop and location-specific potential agricultural worker exposure to extreme humid heat is a necessary early step in the long-term effort to help workers and the agricultural systems they support adapt to climate change, climate variability, and other compound stresses (Raymond *et al* 2020) in a rapidly changing world.

Acknowledgments

The authors would like acknowledge funding for this research supported by NSF awards AGS-1934358, HEGS-2049262, and #1934383. Additional funding for this work was supplied by the Lamont-Doherty Earth Observatory Earth Intern Program at Columbia University.

This project is also supported with funding from the Australian Government under the National Environmental Science Program. The authors would like to thank Tim Cowan and Naomi Benger from the Bureau of Meteorology for providing initial reviews prior to journal submission.

The authors would also like to thank the Smyrna Public Library in Smyrna, GA, where part of this work was completed.

Data availability statement

The data that support the findings of this study are openly available at the following URL/DOI: https://sage.nelson.wisc.edu/data-and-models/datasets/crop-calendar-dataset/.

Data availability statement

The data that support the findings of this study are openly available at the following URLs: ERA5:https://cds.climate.copernicus.eu/#!/search?text=ERA5&type=dataset Global Crop Calendar Dataset:https://sage.nelson.wisc.edu/data-and-models/datasets/crop-calendar-dataset/ Harvested Area Data:http://www.earthstat.org/harvested-area-yield-175-crops/ ENSO ONI: 3 month running mean values available at https://origin.cpc.ncep.noaa.gov/products/analysis_monitoring/ensostuff/ONI_v5.php. Dataset described in Huang *et al* (2017).

Appendix

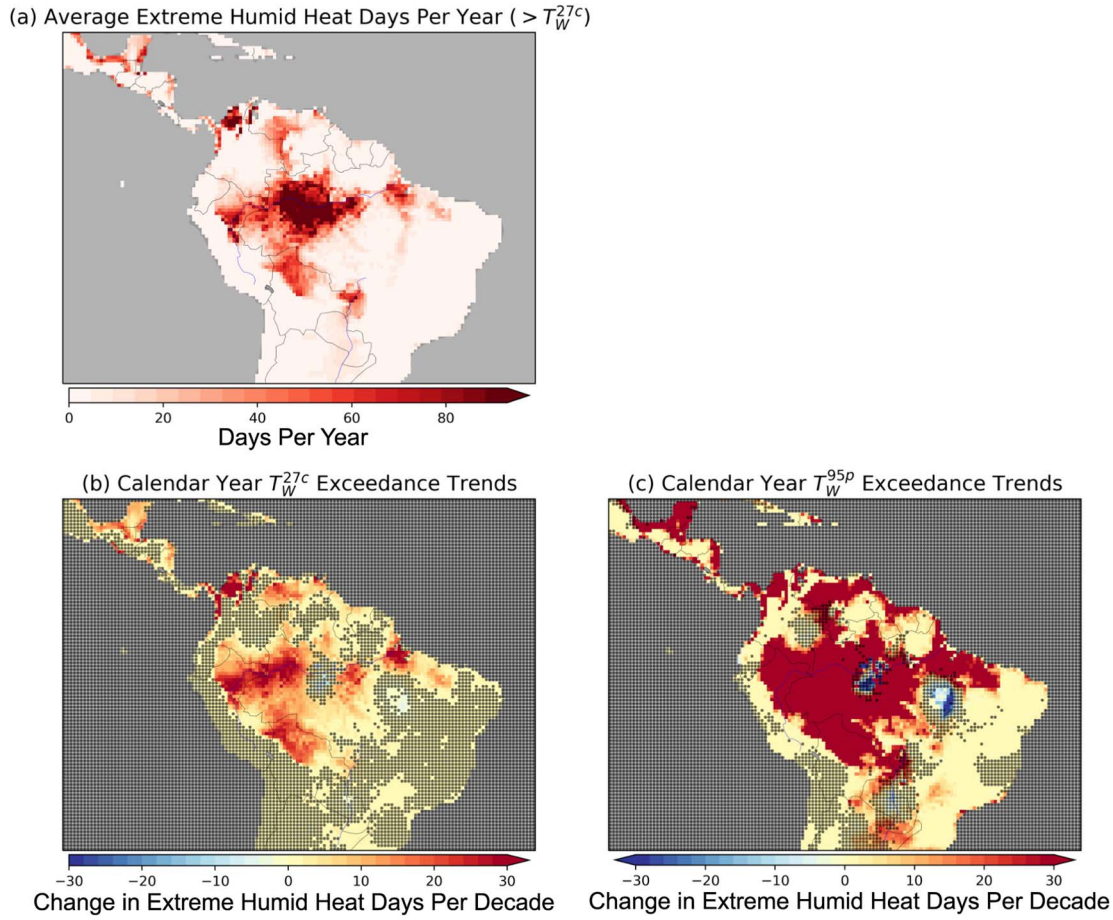

Figure A1. Climatology and trends in extreme humid heat frequencies over Central and South America. (a) Number of days per year exceeding T_W^{27c} over land; note that the color bar saturates at 93 days (~3 months). Linear trends in the number of days per decade exceeding (b) T_W^{27c} and (c) T_W^{95p}. Stippling indicates trends that are not significant at the 95% confidence level using the Mann-Kendall test (p-values <0.001).

Table A1. Breakdown of Global Rice and Maize Cropland Exposure by Season. 'Ratio' refers to the ratio of mean extreme humid heat days ($> T_W^{27c}$) in the planting to harvest seasons for the given crop. Exposed cropland is based on the climatological mean potential worker exposure calculated over the study period (1979–2019).

Cropland area of seasonal humid heat exposure		
	Rice	**Maize**
Total Cropland (km^2)	3.577×10^7	4.345×10^7
Greater Planting Exposure (km^2) (ratio > 1)	7.973×10^6	5.674×10^6
Much Greater Planting Exposure (km^2) (ratio > 2)	5.937×10^6	3.998×10^6
Greater Harvest Exposure (km^2) (ratio < 1)	1.089×10^7	1.223×10^7
Much Greater Harvest Exposure (km^2) (ratio < 0.5)	7.970×10^6	9.551×10^6
Equal Exposure (km^2)	3.642×10^5	4.466×10^5
No Exposure (km^2)	1.654×10^7	2.510×10^7
Greater Planting Exposure (% Total Cropland)	22.3	13.1
Much Greater Planting Exposure (% Total Cropland)	16.6	9.2
Greater Harvest Exposure (% Total Cropland)	30.5	28.1
Much Greater Harvest Exposure (% Total Cropland)	22.3	22.0

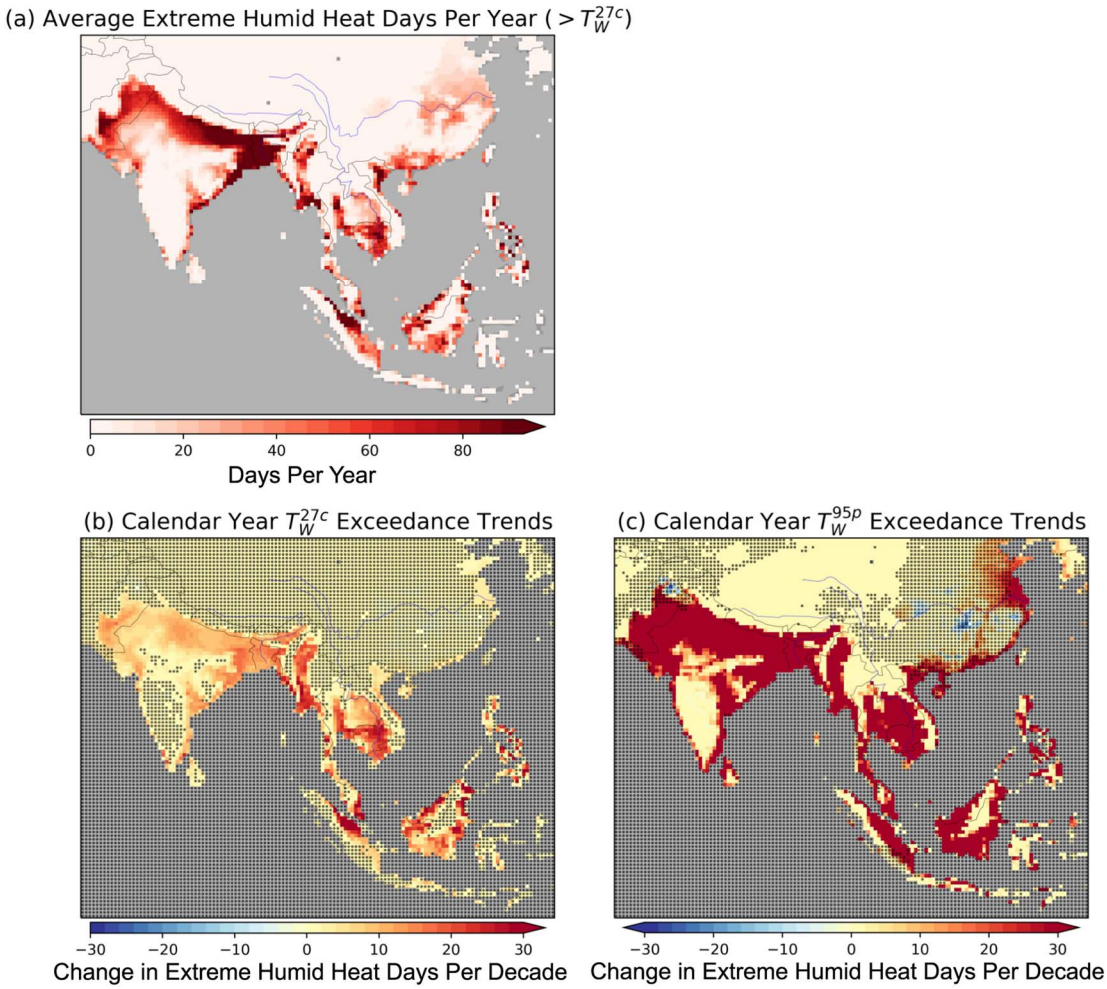

Figure A2. Climatology and trends in extreme humid heat frequencies over South Asia and the Maritime Continent. (a) Number of days per year exceeding T_W^{27c} over land; note that the color bar saturates at 93 days (~3 months). Linear trends in the number of days per decade exceeding (b) T_W^{27c} and (c) T_W^{95p}. Stippling indicates trends that are not significant at the 95% confidence level using the Mann-Kendall test (p-values <0.001).

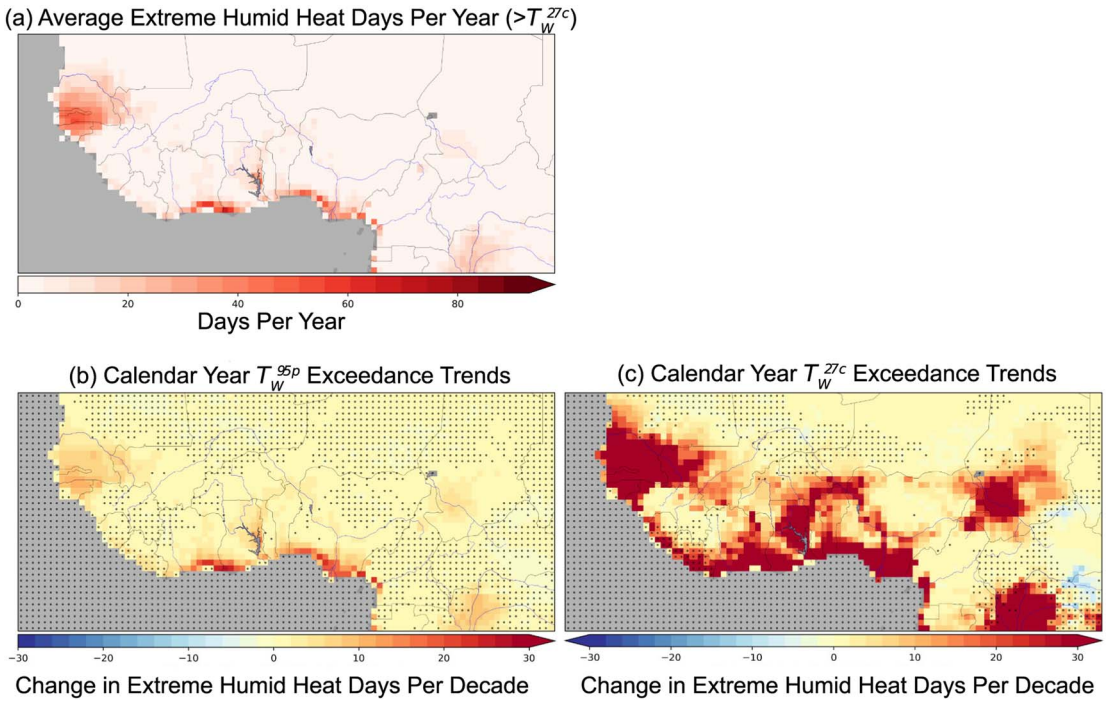

Figure A3. Climatology and trends in extreme humid heat frequencies over the Gulf of Guinea (a) Number of days per year exceeding T_W^{27c} over land; note that the color bar saturates at 93 days (~3 months). Linear trends in the number of days per decade exceeding (b) T_W^{27c} and (c) T_W^{95p}. Stippling indicates trends that are not significant at the 95% confidence level using the Mann-Kendall test (p-values <0.001).

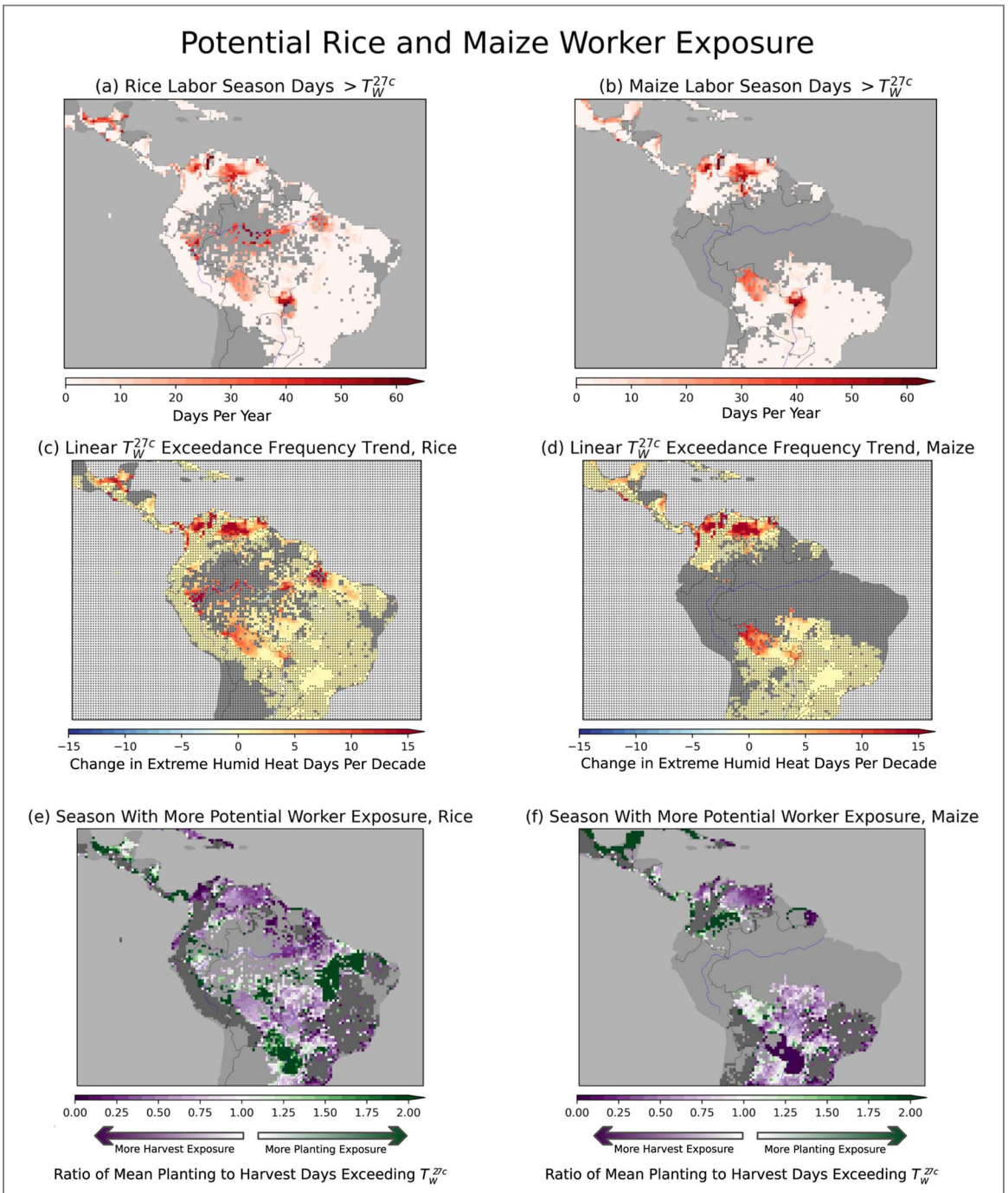

Figure A4. Spatial distribution of potential worker exposure in the labor season for rice and maize in Central and South America. Mean number of extreme humid heat days during the labor season exceeding the absolute threshold T_W^{27c} for (a) rice and (b) maize. Linear trends in the number of labor season days per decade exceeding T_W^{27c} for (c) rice and (d) maize. Stippling shows where trends are not significant using the Mann-Kendall test at the 95% confidence level (p-values < 0.001). Ratio of the mean number of humid heat days exceeding T_W^{27c} in the planting season to those in the harvest season for (e) rice and (f) maize. Values >1 (green, right) show more potential worker exposure in the planting season, values <1 (purple, left) show more potential worker exposure in the harvest season. Areas with no humid heat days in either season are masked in dark grey; areas with no humid heat days in the harvest season, but $\geqslant 1$ day in the planting season are reported as a ratio of >2, where the colorbar saturates.

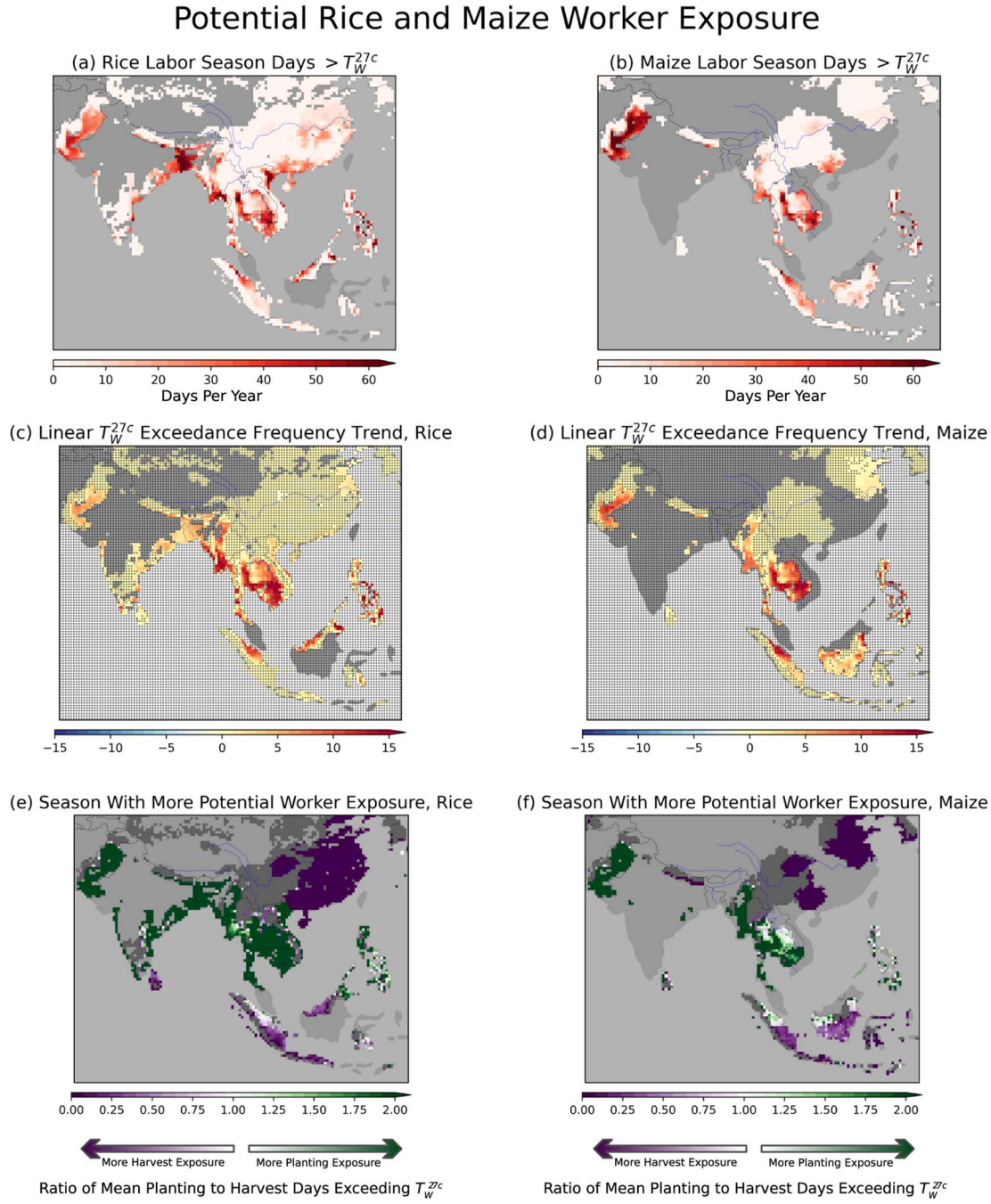

Figure A5. Spatial distribution of potential worker exposure in the labor season for rice and maize in South Asia and the Maritime Continent. Mean number of extreme humid heat days during the labor season exceeding the absolute threshold T_W^{27c} for (a) rice and (b) maize. Linear trends in the number of labor season days per decade exceeding T_W^{27c} for (c) rice and (d) maize. Stippling shows where trends are not significant using the Mann-Kendall test at the 95% confidence level (p-values < 0.001). Ratio of the mean number of humid heat days exceeding T_W^{27c} in the planting season to those in the harvest season for (e) rice and (f) maize. Values >1 (green, right) show more potential worker exposure in the planting season, values <1 (purple, left) show more potential worker exposure in the harvest season. Areas with no humid heat days in either season are masked in dark grey; areas with no humid heat days in the harvest season, but $\geqslant 1$ day in the planting season are reported as a ratio of >2, where the colorbar saturates.

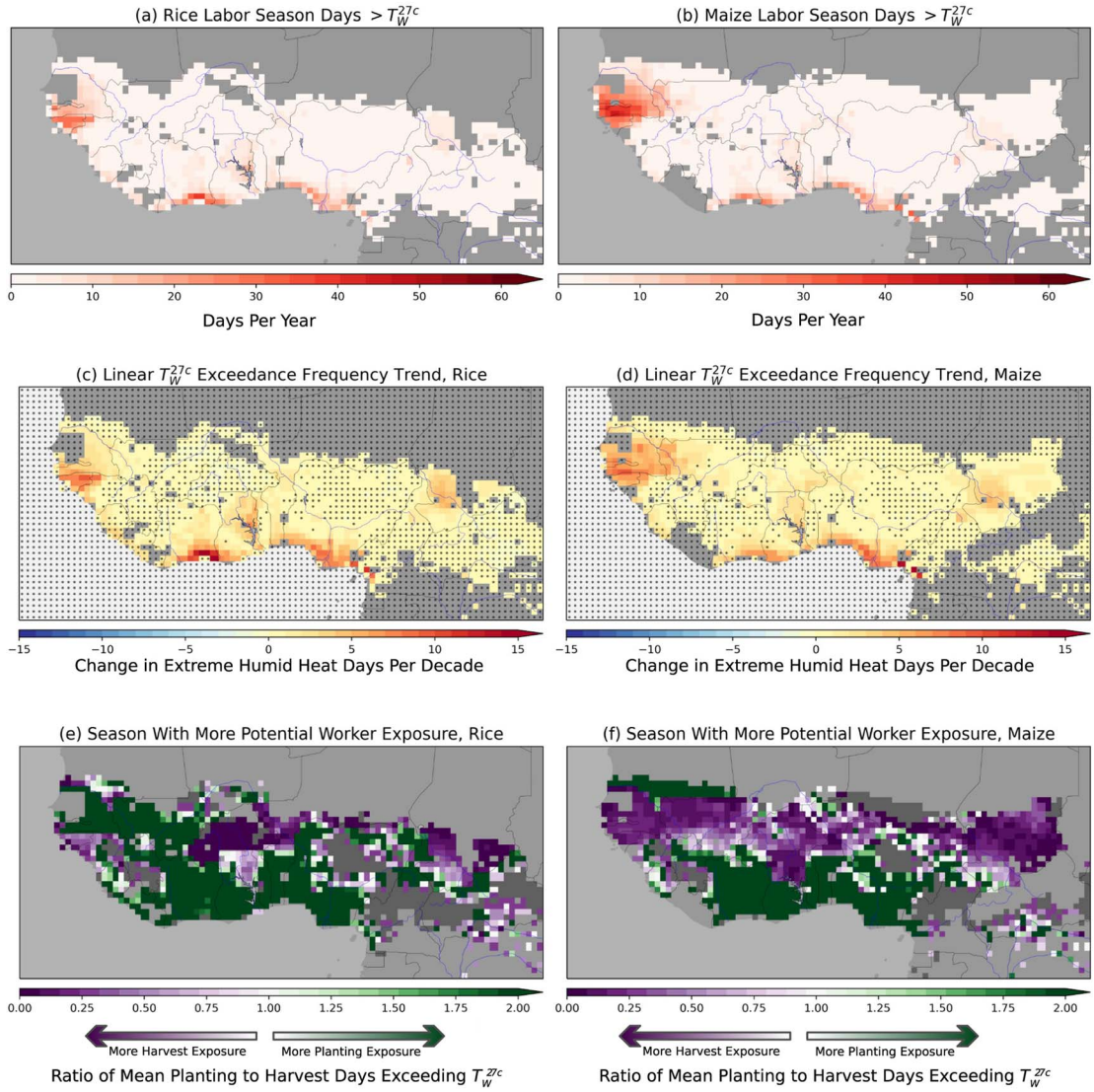

Figure A6. Spatial distribution of potential worker exposure in the labor season for rice and maize in the Gulf of Guinea. Mean number of extreme humid heat days during the labor season exceeding the absolute threshold T_W^{27c} for (a) rice and (b) maize. Linear trends in the number of labor season days per decade exceeding T_W^{27c} for (c) rice and (d) maize. Stippling shows where trends are not significant using the Mann-Kendall test at the 95% confidence level (p-values < 0.001). Ratio of the mean number of humid heat days exceeding T_W^{27c} in the planting season to those in the harvest season for (e) rice and (f) maize. Values >1 (green, right) show more potential worker exposure in the planting season, values <1 (purple, left) show more potential worker exposure in the harvest season. Areas with no humid heat days in either season are masked in dark grey; areas with no humid heat days in the harvest season, but $\geqslant 1$ day in the planting season are reported as a ratio of >2, where the colorbar saturates.

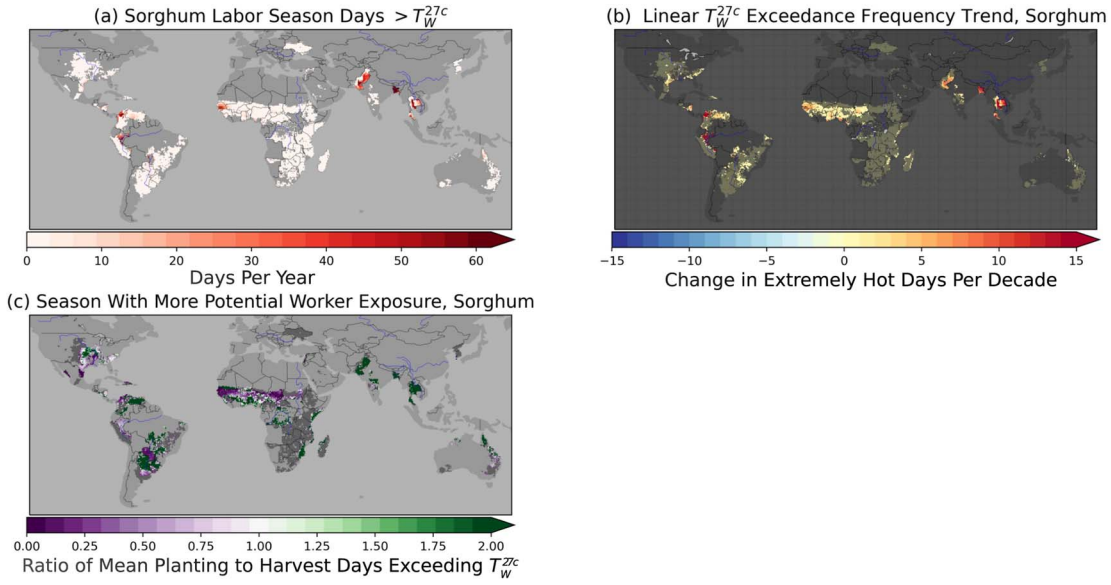

Figure A7. Spatial distribution of potential worker exposure in the labor season for sorghum. (a) Mean number of extreme humid heat days during the labor season exceeding the absolute threshold T_W^{27c}. (b) Linear trends in the number of labor season days per decade exceeding T_W^{27c}. Hatching shows where trends are not significant using the Mann-Kendall test at the 95% confidence level (p-values < 0.001). (c) Ratio of the mean number of humid heat days exceeding T_W^{27c} in the planting season to those in the harvest season. Values >1 (green, right) show more potential worker exposure in the planting season, values <1 (purple, left) show more potential worker exposure in the harvest season. Areas with no humid heat days in either season are masked in dark grey; areas with no humid heat days in the harvest season, but $\geqslant 1$ day in the planting season are reported as a ratio of >2, where the colorbar saturates.

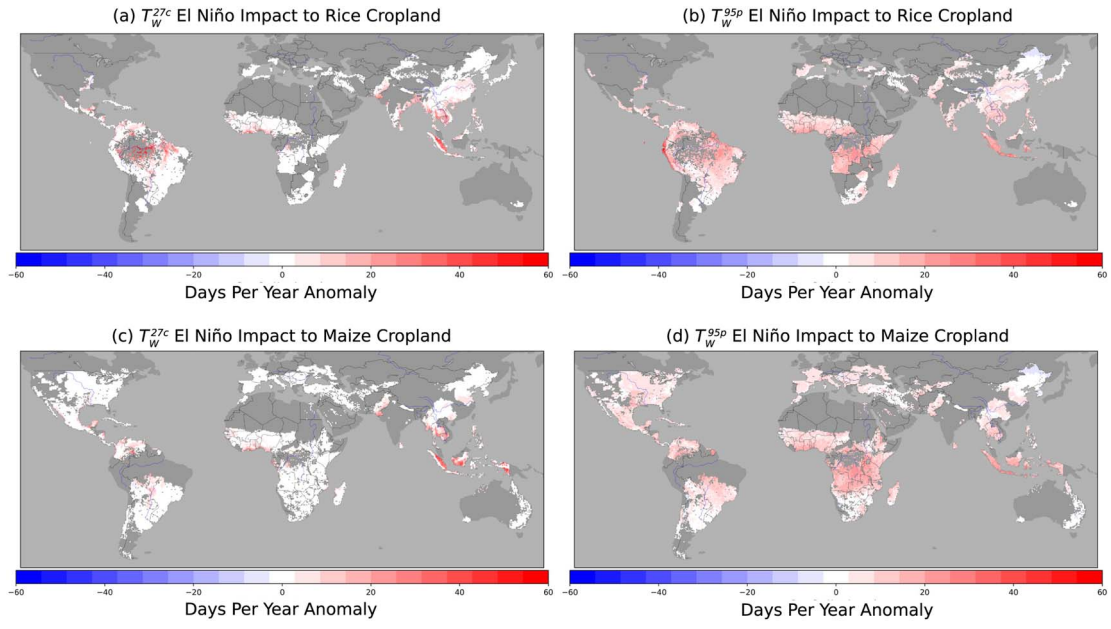

Figure A8. Mean humid heat frequency anomalies during El Niño events over rice and maize cropland. Composites of the anomalous annual number of extreme humid heat days for T_W^{27c} over (a) rice cropland (c) maize cropland and T_W^{95p} over (b) rice cropland and (d) maize cropland, during years with moderate to very strong ONI El Niño events (1983, 1987, 1988, 1992, 1995, 1998, 2003, 2010, and 2016). Composites are calculated after removing background linear trends in extreme humid heat day frequencies. Composites are produced using data for the entire calendar year.

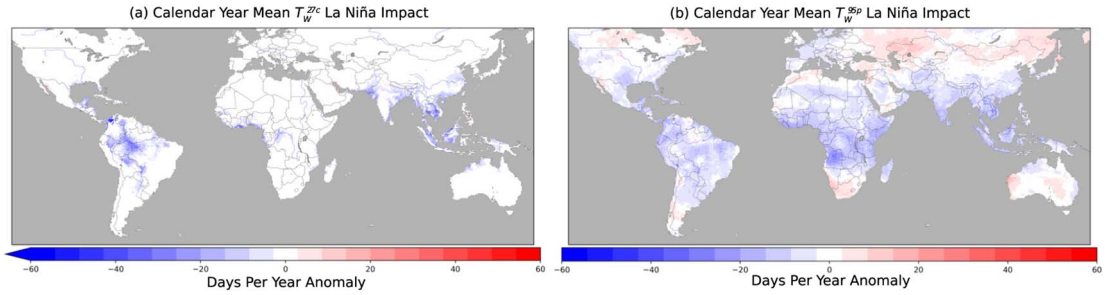

Figure A9. Mean humid heat frequency anomalies during La Niña events. Composites of the anomalous annual number of extreme humid heat days for (a) T_W^{27c} and (b) T_W^{95p}, during years with moderate to very strong ONI La Niña events (1989, 1996, 1999, 2000, 2008, 2011, and 2012). La Niña years are considered the latter year of a two-year event, as for El Niño events analyzed in the main text. Composites are calculated after removing background linear trends in extreme humid heat day frequencies. Composites are produced using data for the entire calendar year.

ORCID iDs

Connor D Diaz https://orcid.org/0009-0004-3516-6008
Deepti Singh https://orcid.org/0000-0001-6568-435X
Cassandra D W Rogers https://orcid.org/0000-0003-3752-7378
Ethan Coffel https://orcid.org/0000-0003-3172-467X

References

Buzan J R, Oleson K and Huber M 2015 Implementation and comparison of a suite of heat stress metrics within the Community Land Model version 4.5 *Geoscientific Model Development* **8** 151–70
Climate Adaptation Action Plan: October 2021 *U.S. Environmental Protection Agency* https://epa.gov/system/files/documents/2021-09/epa-climate-adaptation-plan-pdf-version.pdf
Coffel E, Horton R M and de Sherbinin A 2017 Temperature and humidity based projections of a rapid rise in global heat stress exposure during the XXI century *Environ. Res. Lett.* **13** 014001
Davies-Jones R 2008 An effcient and accurate method for computing thewet-bulb temperature along pseudoadiabats *Mon. Weather Rev.* **136** 2764–85
de Lima C Z, Buzan J R, Moore F C, Baldos U L C, Huber M and Hertel T W 2021 Heat stress on agricultural workers exacerbates crop impacts of climate change *Environ. Res. Lett.* **16** 044020
Deryng D, Conway D, Ramankutty N, Price J and Warren R 2014 Global crop yield response to extreme heat stress under multiple climate change futures *Environ. Res. Lett.* **9** 034011
Ergon Associates 2016 *Addressing worker vulnerability in agricultural and food supply chains: Pilot toolkit* Ethical Trading Initiative https://ethicaltrade.org/sites/default/files/shared_resources/vulnerable_workers_toolkit.pdf
Forzieri G, Bianchi A, Silva F B E, Marin Herrera M A, Leblois A, Lavalle C, Aerts J C and Feyen L 2018 Escalating impacts of climate extremes on critical infrastructures in Europe *Global Environ. Change* **48** 97–107
Gourdji S M, Sibley A M and Lobell D B 2013 Global crop exposure to critical high temperatures in the reproductive period: historical trends and future projections *Environ. Res. Lett.* **8** 024041
Hanna E G and Tait P W 2015 Limitations to thermoregulation and acclimatization challenge human adaptation to global warming *Internatioanl Journal of Environmental Research and Public Health* **12** 8034–74
Hersbach H, Bell B, Berrisford P, Hirahara S and Horáanyi A 2020 The ERA5 global reanalysis *Q. J. R. Meteorolog. Soc.* **146** 1999–2049
Huang B, Thorne P W, Banzon V F, Boyer T, Chepurin G, Lawrimore J H, Menne M J, Smith T M, Vose R S and Zhang H-M 2017 NOAA extended reconstructed sea surface temperature (ERSST), version 5. *NOAA National Centers for Environmental Information* **V.5** NCEI DSI 3649_04
Iizumi T and Ramankutty N 2016 Changes in yield variability of major crops for 1981-2010 explained by climate change *Environ. Res. Lett.* **11** 034003
Kang S and Eltahir E A 2018 North China Plain threatened by deadly heatwaves due to climate change and irrigation *Nat. Commun.* **9** 2894
Kopp B (2020) *WetBulb.m.* https://github.com/bobkopp/WetBulb.m
Krakauer N Y, Cook B I and Puma M J 2020 Effect of irrigation on humid heat extremes *Environ. Res. Lett.* **15** 094010
Mac V V T and McCauley L A 2017 Farmworker vulnerability to heat hazards: A conceptual framework *Journal of Nursing Scholarship* **49** 617–24
Mishra V, Ambika A K, Asoka A, Aadhar S, Buzan J, Kumar R and Huber M 2020 Moist heat stress extremes in India enhanced by irrigation *Nat. Geosci.* **13** 722–8
Monfreda C, Ramankutty N and Foley J A 2008 Farming the planet: 2. geographic distribution of crop areas, yields, physiological types, and net primary production in the year 2000 *Global Biogeochem. Cycles* **22** GB1022
Monteiro J M and Caballero R 2019 Characterization of extreme wet-bulb temperature events in southern Pakistan *Geophys. Res. Lett.* **46** 10659–68
National Weather Service (n.d.). Heat forecast tools [National weather service]. https://weather.gov/safety/heat-index
Osilla E V, Marsidi J L and Sharma S 2022 *Physiology, Temperature Regulation* (StatPearls Publishing) http://europepmc.org/books/NBK507838

Potapov P, Turubanova S, Hansen M C, Tyukavina A, Zalles V, Khan A, Song X-P, Pickens A, Shen Q and Cortez J 2021 Global maps of cropland extent and change show accelerated cropland expansion in the twenty-first century *Nature Food* **3** 19–28

Ranasinghe R *et al* 2021 Climate change information for regional impact and for risk assessment *Climate Change 2021: The Physical Science Basis. Contribution of Working Group I to The Sixth Assessment Report of The Intergovernmental Panel on Climate Change* ed V Masson-Delmotte *et al* (Cambridge University Press) pp 1767–926

Raymond C, Matthews T and Horton R M 2020 The emergence of heat and humidity too severe for human tolerance *Science Advances* **6** eaaw1838

Raymond C, Suarez-Gutierrez L, Kornhuber K, Pascolini-Campbell M, Sillmann J and Waliser D E 2022 Increasing spatiotemporal proximity of heat and precipitation extremes in a warming world quantified by a large model ensemble *Environ. Res. Lett.* **17** 035005

Riley K, Wilhalme H, Delp L and Eisenman D P 2018 Mortality and morbidity during extreme heat events and prevalence of outdoor work: an analysis of community-level data from Los Angeles County, California *International Journal of Environmental Research and Public Health* **15** 580

Rogers C D W, Ting M, Li C, Kornhuber K, Coffel E D, Horton R M, Raymond C and Singh D 2021 Recent increases in exposure to extreme humid-heat events disproportionately affect populated regions *Geophys. Res. Lett.* **48** e2021GL094183

Sacks W J, Deryng D, Foley J A and Ramankutty N 2010 Crop planting dates: an analysis of global patterns *Global Ecol. Biogeogr.* **19** 607–20

Simon M F and Garagorry F L 2005 The expansion of agriculture in the Brazilian Amazon *Environ. Conserv.* **32** 203–12

Sherwood S C and Huber M 2010 An adaptability limit to climate change due to heat stress *PNAS* **107** 9552–5

Spector J T, Bonauto D K, Sheppard L, Busch-Isaksen T, Calkins M, Adams D, Lieblich M and Fenske R A 2016 A case-crossover study of heat exposure and injury risk in outdoor agricultural workers *PLoS One* **11** e0164498

Sun X, Renard B, Thyer M, Westra S and Lang M 2015 A global analysis of the asymmetric effect of ENSO on extreme precipitation *J. Hydrol.* **530** 51–65

Thiery W, Davin E L, Lawrence D M, Hirsch A L, Hauser M and Seneviratne S I 2017 Present-day irrigation mitigates heat extremes *Journal of Geophysical Research: Atmospheres* **122** 1403–22

Tigchelaar M, Battisti D S and Spector J T 2020 Work adaptations insuffcient to address growing heat risk for U.S. agricultural workers *Environ. Res. Lett.* **15** 094035

Ting M, Lesk C, Liu C, Li C, Horton R M, Coffel E D, Rogers C D W and Singh D 2023 Contrasting impacts of dry versus humid heat on US corn and soybean yields *Sci. Rep.* **13** 710

Vecellio D J, Wolf S T, Cottle R M and Kenney W L 2021 Evaluating the 35 °C wet-bulb temperature adaptability threshold for young, healthy adults (PSU HEAT) *J. Appl. Physiol.* **132** 340–5

Wang P, Yang Y, Tang J, Leung L R and Liao H 2020 Intensified humid heat events under global warming *Geophys. Res. Lett.* **48** e2020GL091462

Wesseling C *et al* 2020 Chronic kidney disease of non-traditional origin in Mesoamerica: A disease primarily driven by occupational heat stress *Pan American Journal of Public Health* **44** e15